

Dark matter and B -meson anomalies in a flavor dependent gauge symmetry

Parada T. P. Hutaurok,^{1,*} Takaaki Nomura,^{2,†} Hiroshi Okada,^{1,‡} and Yuta Orikasa^{3,§}

¹*Asia Pacific Center for Theoretical Physics, Pohang, Gyeongbuk 37673, Korea*

²*School of Physics, KIAS, Seoul 02455, Korea*

³*Institute of Experimental and Applied Physics, Czech Technical University, Prague 12800, Czech Republic*

(Dated: March 12, 2019)

A possibility of explaining the anomalies in the semileptonic B -meson decay $B \rightarrow K^* \mu \bar{\mu}$ has been explored in the framework of the gauged $U(1)_{\mu-\tau}$ symmetry. Apart from the muon anomalous magnetic moment and neutrino sector, we formulate the model starting with a valid Lagrangian and consider the constraints from the neutral meson mixings, the bounds on direct detection and the relic density of the bosonic dark matter candidate augmented to collider constraints. We search the parameter space, which accommodate the size of the anomaly of the $B \rightarrow K^* \mu \bar{\mu}$ decay, to satisfy all experimental constraints. We found the allowed region on the plane of the dark matter and Z' masses is rather narrow compared to the previous analysis.

I. INTRODUCTION

A flavor dependent gauge symmetry is one of the promising candidates for new physics to describe the anomalies and other phenomenologies related with the flavor physics as well as to ensure the dark matter (DM) stability. In particular, the model of $U(1)_{\mu-\tau}$ provides several phenomenological prescriptions to resolve, namely, muon anomalous magnetic moment [1], ¹ experimental anomalies of semileptonic B -meson decay [2, 3], neutrino sector [4–15], and other related topics [16, 17]. Among them, the B -meson decay anomaly is a very challenging topic due to some indications of new physics have been suggested in the B physics. For example, the angular observable P'_5 in the decay of the B meson $B \rightarrow K^* \mu^+ \mu^-$ [28] has been measured with deviation of 3.4σ from the integrated luminosity of 3.0 fb^{-1} at the LHCb [18] which confirms the previous result with deviation of 3.7σ [19]. In addition, the same observable were measured by Belle collaboration [20, 21] with the deviation of 2.1σ . Furthermore, an anomaly in the measurement of the ratio of branching fraction $R_K = BR(B^+ \rightarrow K^+ \mu^+ \mu^-)/BR(B^+ \rightarrow K^+ e^+ e^-)$ [22, 23] at the LHCb indicates a deviation of 2.6σ from the lepton universality predicted in the standard model (SM) [24]. Recently, the LHCb collaboration has also measured the ratio of $R_{K^*} = BR(B \rightarrow K^* \mu^+ \mu^-)/BR(B \rightarrow K^* e^+ e^-)$ which is found to be deviated from the SM prediction by $\sim 2.4\sigma$ as $R_{K^*} = 0.660^{+0.110}_{-0.070} \pm 0.024(0.685^{+0.113}_{-0.069} \pm 0.047)$ for $(2m_\mu^2) < q^2 < 1.1 \text{ GeV}^2$ ($1.1 \text{ GeV}^2 < q^2 < 6 \text{ GeV}^2$) [25].

In previous study of Ref. [2], we have proposed the flavor dependent gauge symmetry. This has successfully explained the anomaly of $B \rightarrow K^* \ell^+ \ell^-$ decay through generating the

flavor violating Z' boson interactions at one loop level. In the model, the only Wilson coefficient C_9 with μ and τ in the B decays are generated via extra Z' boson exchange, but this is explicitly not applicable for $B \rightarrow K^* e \bar{e}$ process [28]. We have also included a bosonic DM χ candidate and the vectorlike exotic quarks Q'_a , which are needed to generate the Wilson coefficient C_9 at one loop level. Thus the DM relic density [29] can be explained the measured anomalies in decay of $B \rightarrow K^* \ell^+ \ell^-$ via s-channel process mediated by Z' boson exchange [30, 31], where Z' boson exchange can avoid a conflict with the constraints from the spin independent DM direct detection searches such as experiments of LUX [32] and XENON1t [33].

In this paper, we adopt the flavor dependent gauge symmetry model with more complete manner. We then perform a more detailed analysis in which we take into account the decay width of the Z' boson which is related with the relic density of the DM, the constraints from the spin independent DM-nucleon elastic scattering cross section mediated by the vectorlike quarks Q'_a at tree level, the large electron-positron (LEP) collider, and the large hadron collider (LHC), to improve the previous analyses of Ref. [2]. In our present numerical analysis, we find that the allowed regions of the DM and Z' masses are narrower than that of the previous analysis. This is expected due to the decay width of Z' is rather larger.

This letter is organized as follows. In Sec. II, we briefly introduce a valid Lagrangian of our model including the Higgs potential with the inert conditions, the B -meson anomaly, the collider physics, and the neutral meson mixings. A brief comment on how to directly produce the exotic quarks, and the experimental constraints of the DM are also presented. In Sec. III, we present our numerical analysis results. Finally Sec. IV is devoted to the summary of our results and conclusions.

II. MODEL SETUP AND CONSTRAINTS

*Electronic address: parada.hutaurok@apctp.org

†Electronic address: nomura@kias.re.kr

‡Electronic address: hiroshi.okada@apctp.org

§Electronic address: Yuta.Orikasa@utef.cvut.cz

¹ Recently, a stringent constraint of the neutrino-trident process gives narrower parameter spaces of the extra gauge coupling (g') and mass ($m_{Z'}$).

In this section, we present a formulation of our model. We briefly introduce a gauged $U(1)_{\mu-\tau}$ symmetry with three families of the vectorlike isospin doublet quarks Q'_a , an isospin singlet inert complex boson χ , and singlet boson φ with nonzero vacuum expectation value (VEV) which is denoted by $\langle\varphi\rangle \equiv v_\varphi/\sqrt{2}$, where H is the SM Higgs and its VEV is denoted by $\langle H\rangle \equiv v_H/\sqrt{2}$. The charge assignments of these new fermion and boson fields are summarized in Tables I and II, respectively.

A relevant Lagrangian under these symmetries is defined by

$$-\mathcal{L} = y_{\ell_i} \bar{L}_{Li} H e_{Ri} + f_{aj} \overline{Q'_{Ra}} Q_{Lj} \chi + M_a \bar{Q}'_a Q'_a + \text{h.c.}, \quad (1)$$

where $a = 1 - 3$ and $(i, j) = e, \mu, \tau$ are generation indices, and the quark sector Q_{Lj} is same as the SM. Note that the charged-lepton sector is diagonal due to the $U(1)_{\mu-\tau}$ symmetry.

Higgs potential is given by

$$V = m_H^2 |H|^2 + m_\varphi^2 |\varphi|^2 + m_\chi^2 |\chi|^2 + \frac{1}{4} \lambda_H |H|^4 + \frac{1}{4} \lambda_\varphi |\varphi|^4 + \frac{1}{4} \lambda_\chi |\chi|^4 + \lambda_{H\varphi} |H|^2 |\varphi|^2 + \lambda_{H\chi} |H|^2 |\chi|^2 + \lambda_{\varphi\chi} |\varphi|^2 |\chi|^2, \quad (2)$$

where each field is defined to be

$$H = \begin{pmatrix} h^+ \\ \frac{1}{\sqrt{2}}(v_H + h + iz) \end{pmatrix}, \quad \varphi = \frac{1}{\sqrt{2}}(v_\varphi + \varphi_R + iz'), \quad (3)$$

where h^+ , z , and z' are respectively absorbed by the gauged bosons; W^+ , Z , and Z' . After inserting the tadpole conditions for H and φ , the CP-even mass matrix is obtained as

$$M_{even}^2 = \begin{pmatrix} v_H^2 \lambda_H & 2v_H v_\varphi \lambda_{H\varphi} \\ 2v_H v_\varphi \lambda_{H\varphi} & v_\varphi^2 \lambda_\varphi \end{pmatrix}. \quad (4)$$

After the diagonalization, the mass eigenvalues and eigenstates

TABLE II: Field contents of bosons and their charge assignments under $SU(2)_L \times U(1)_Y \times U(1)_{\mu-\tau}$, where $q_{x,y} \neq 0$, $SU(3)_C$ singlet for all bosons, and χ is a complex boson which is considered as a DM candidate. Hence $q_y \neq \pm q_x$, $q_y \neq \pm 2q_x$, and $q_x \neq \pm 3q_y$ are simultaneously satisfied.

	VEV $\neq 0$		Inert
Bosons	H	φ	χ
$SU(2)_L$	2	1	1
$U(1)_Y$	$\frac{1}{2}$	0	1
$U(1)_{\mu-\tau}$	0	q_y	q_x

are respectively given by

$$OM_{even}^2 O^T = \begin{pmatrix} c_\theta & -s_\theta \\ s_\theta & c_\theta \end{pmatrix} \begin{pmatrix} v_H^2 \lambda_H & 2v_H v_\varphi \lambda_{H\varphi} \\ 2v_H v_\varphi \lambda_{H\varphi} & v_\varphi^2 \lambda_\varphi \end{pmatrix} \begin{pmatrix} c_\theta & s_\theta \\ -s_\theta & c_\theta \end{pmatrix} = \text{diag}(m_{h_{SM}}^2, m_H^2), \quad (5)$$

$$m_{h_{SM}}^2 = \frac{1}{2} \left(A - \sqrt{(v_\varphi^2 \lambda_\varphi - v_H^2 \lambda_H)^2 + 16v_\varphi^2 v_H^2 \lambda_{H\varphi}^2} \right),$$

$$m_H^2 = \frac{1}{2} \left(A + \sqrt{(v_\varphi^2 \lambda_\varphi - v_H^2 \lambda_H)^2 + 16v_\varphi^2 v_H^2 \lambda_{H\varphi}^2} \right),$$

where $A = v_\varphi^2 \lambda_\varphi + v_H^2 \lambda_H$, $\sin \theta (\cos \theta) \equiv c_\theta (s_\theta)$, and $\tan \theta \equiv t_\theta$ satisfies the following relation:

$$2v_H v_\varphi \lambda_{H\varphi} t_\theta^2 - (v_\varphi^2 \lambda_\varphi - v_H^2 \lambda_H) t_\theta - 2v_H v_\varphi \lambda_{H\varphi} = 0. \quad (6)$$

The mass eigenvalue of χ is given by

$$m_\chi^2 = v_\varphi^2 \lambda_{\varphi\chi} + v_H^2 \lambda_{H\chi} + 2m_\chi^2. \quad (7)$$

The inert conditions for χ are given by

$$\begin{aligned} \lambda_H, \lambda_\varphi, \lambda_\chi, \lambda_{H\varphi}, \lambda_{H\chi}, \lambda_{\varphi\chi} &> 0, \\ m_\chi^2 &> 0, \\ \lambda_H \lambda_\varphi &> 4\lambda_{H\varphi}^2. \end{aligned} \quad (8)$$

Z' boson: We have Z' boson from $U(1)_{\mu-\tau}$ gauge symmetry. After φ develops its VEV, the mass of Z' boson is generated as

$$m_{Z'} = q_y^2 g'^2 v_\varphi^2, \quad (9)$$

where g' is a gauge coupling for $U(1)_{\mu-\tau}$. The gauge interactions among Z' and fermions are given by

$$\begin{aligned} \mathcal{L} \supset g' Z'_\mu (\bar{L}_{L\mu} \gamma^\mu L_{L\mu} - \bar{L}_{L\tau} \gamma^\mu L_{L\tau} + \bar{\mu}_R \gamma^\mu \mu_R \\ - \bar{\tau}_R \gamma^\mu \tau_R + q_y \sum_{a=1}^3 \bar{Q}'_a \gamma^\mu Q'_a). \end{aligned} \quad (10)$$

Note that we ignore the kinetic mixing effects between $U(1)_{\mu-\tau}$ and $U(1)_Y$ by assuming the contributions is relatively very small.

Explanation of the anomaly in $B \rightarrow K^{(*)} \ell^+ \ell^-$ decay: In our case, we have a Wilson coefficient C_9 , which is associated

TABLE I: Field contents of fermions and their charge assignments under $SU(2)_L \times U(1)_Y \times U(1)_{\mu-\tau}$, where $q_x \neq 0$ and the lower index a of Q' is the number of family which runs over 1 - 3.

	Leptons						Exotic vector fermions
Fermions	L_{Le}	$L_{L\mu}$	$L_{L\tau}$	e_R	μ_R	τ_R	Q'_a
$SU(3)_C$	1	1	1	1	1	1	3
$SU(2)_L$	2	2	2	1	1	1	2
$U(1)_Y$	$-\frac{1}{2}$	$-\frac{1}{2}$	$-\frac{1}{2}$	-1	-1	-1	$\frac{1}{6}$
$U(1)_{\mu-\tau}$	0	1	-1	0	1	-1	q_x

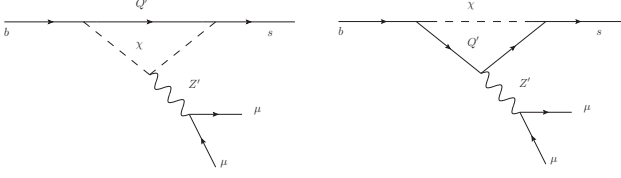


FIG. 1: The diagrams introduces an effective coupling for $Z'_\mu \bar{b} \gamma^\mu s + h.c.$ interaction.

with $(\bar{s} \gamma_\mu P_L b)(\mu \gamma^\mu \mu)$, via Fig. 1. Then their contribution to a Wilson coefficient $\Delta C_9^{\mu\mu}$ is given by [2, 28]

$$\Delta C_9^{\mu\mu} \simeq \frac{q_x g'^2}{(4\pi)^2 m_{Z'}^2 C_{\text{SM}}} \sum_{a=1}^3 f_{3a}^\dagger f_{a2} \int [dx] \ln \left(\frac{\Delta[M_a, m_\chi]}{\Delta[m_\chi, M_a]} \right),$$

$$C_{\text{SM}} \equiv \frac{V_{tb} V_{ts}^* G_F \alpha_{\text{em}}}{\sqrt{2} \pi}, \quad (11)$$

$$\Delta[m_1, m_2] = (x + y - 1)(x m_b^2 + y m_s^2) + x m_1^2 + (y + z) m_2^2,$$

where $[dx] \equiv \int_0^1 dx dy dz \delta(1 - x - y - z)$, V_{tb} , V_{ts} are the 3-3 and 3-2 elements of the Cabibbo-Kobayashi-Maskawa (CKM) matrix, respectively, $G_F \approx 1.17 \times 10^{-5} [\text{GeV}]^{-2}$ is the Fermi constant, $\alpha_{\text{em}} \approx 1/137$ is the electromagnetic fine-structure constant, and $m_b \approx 4.18 \text{ GeV}$ and $m_s \approx 0.095 \text{ GeV}$ are the bottom and strange quark masses, respectively, which are given by the $\overline{\text{MS}}$ renormalization scheme at a scale $\mu = 2 \text{ GeV}$ [34]. We assume $m_b, m_s \ll m_{Z'}$ in Eq. (11). m_χ and M_a are respectively χ and Q'_a masses. We use the global fit for the value of C_9 [35], which gives the best fit value of $\Delta C_9 \approx -1.09$. The possible values of the ΔC_9 are respectively obtained as

$$\Delta C_9 = [-1.29, -0.87] \text{ for } 1\sigma, \quad [-1.67, -0.39] \text{ for } 3\sigma. \quad (12)$$

Constraint from K -meson decay: Here we discuss a constraint from K -meson decay. Considering a small effect of the charge parity (CP) violation emerges from new physics, the strongest bound is derived by $K_S \rightarrow \pi^0 \mu \bar{\mu}$ decay. It is then induced by the effective Hamiltonian [26, 27]

$$H_{\text{eff}} = -\frac{G_F}{\sqrt{2}} V_{ud} V_{us}^* C_{7V}^{\mu\mu} (\bar{s} \gamma^\mu (1 - \gamma_5) d) (\bar{\mu} \gamma_\mu \mu). \quad (13)$$

Similar to the Wilson coefficient C_9 case, the Wilson coefficient ΔC_{7V} arising from the Z' exchange can be induced at one loop level. We then obtain

$$\Delta C_{7V}^{\mu\mu} \simeq \frac{q_x g'^2}{(4\pi)^2 m_{Z'}^2} \frac{1}{\sqrt{2} G_F V_{ud} V_{us}^*}$$

$$\times \sum_{a=1}^3 f_{2a}^\dagger f_{a1} \int [dx] \ln \left(\frac{\Delta[M_a, m_\chi]}{\Delta[m_\chi, M_a]} \right). \quad (14)$$

The values of the experimental constraint is given by [26]

$$|a_S^{\mu\mu}| = 1.54_{-0.32}^{+0.40}, \quad a_S^{\mu\mu} \equiv \frac{2\pi}{\alpha_{\text{em}}} V_{ud} V_{us}^* C_{7V}^{\mu\mu}, \quad (15)$$

where a large uncertainty is found. For estimating the Z' contribution, we derive

$$\Delta a_S^{\mu\mu} \simeq 0.46 \left(\frac{g'}{0.1} \right)^2 \left(\frac{100 \text{ GeV}}{m_{Z'}} \right)^2$$

$$\times \sum_{a=1}^3 f_{2a}^\dagger f_{a1} \int [dx] \ln \left(\frac{\Delta[M_a, m_\chi]}{\Delta[m_\chi, M_a]} \right). \quad (16)$$

We find that $\Delta a_S^{\mu\mu}$ sufficiently lies within the range of the experimental uncertainty if the Yukawa coupling f is taken $O(0.1)$ and the constraint from Δm_K tends to be stronger.

LHC constraint: Since we consider no interactions between the electron-positron pair and Z' , we evade the stringent constraint from the LEP experiment. However, we need a constraint from the experiment of LHC, while we consider interactions among u and d quarks via one-loop contributions, as it can be explicitly seen in the part of $b \rightarrow s \ell \bar{\ell}$.

The most stringent constraint from the LHC arises from the process of $q \bar{q} \rightarrow Z' \rightarrow \bar{\mu} \mu$. From this constraint, the effective mass bound suggests $30 \text{ TeV} \lesssim \Lambda$, where its effective operator is given by $\frac{1}{\Lambda^2} (\bar{q} \gamma_\mu P_L q) (\bar{\mu} \gamma^\mu P_L \mu)$ [36]. We then can easily estimate the bound on $m_{Z'}$ in the effective operator analysis. Similar to the case of $b \rightarrow s \bar{\mu} \mu$, our effective operator is defined as

$$\mathcal{L} \simeq \frac{q_x g'^2}{(4\pi)^2 m_{Z'}^2} \sum_{a=1}^3 f_{1a}^\dagger f_{a1} \int [dx] \ln \left(\frac{x M_a^2 + (y + z) m_\chi^2}{x m_\chi^2 + (y + z) M_a^2} \right)$$

$$\times (\bar{q} \gamma_\mu P_L q) (\bar{\mu} \gamma^\mu P_L \mu), \quad (17)$$

where $q = (u, d)$. It implies that we have the following constraint from the LHC:

$$\frac{m_{Z'}}{g'} \gtrsim 30 \left[\frac{q_x}{(4\pi)^3} \sum_{a=1}^3 f_{1a}^\dagger f_{a1} \int [dx] \ln \left(\frac{x M_a^2 + (y + z) m_\chi^2}{x m_\chi^2 + (y + z) M_a^2} \right) \right]^{\frac{1}{2}}$$

$$\times \text{TeV}. \quad (18)$$

When we take a degenerate mass for M_a as 1000 GeV and $m_\chi = 100 \text{ GeV}$, the constraint then gives

$$\frac{m_{Z'}}{g'} \gtrsim 0.45 \left[\sum_{a=1}^3 f_{1a}^\dagger f_{a1} \right]^{\frac{1}{2}} \text{TeV}. \quad (19)$$

This shows that the constraint can be easily avoided while the coupling f_{1a} is not too large.

$M - \bar{M}$ mixing: The neutral meson mixings also give the constraints of the parameter space. The neutral meson mixings are shown in Fig. 2 and their formulas be lower than the ex-

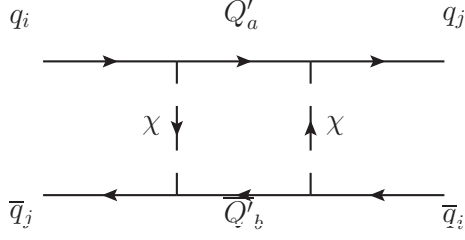


FIG. 2: The diagram representing the neutral meson mixings.

perimental bounds as follows [34, 37]:

$$\Delta m_K \approx \sum_{a,b=1}^3 f_{2a}^\dagger f_{a1} f_{2b}^\dagger f_{b1} F_{box}^K[M_a, M_b] \lesssim 3.48 \times 10^{-15} \text{ [GeV]}, \quad (20)$$

$$\Delta m_{B_d} \approx \sum_{a,b=1}^3 f_{3a}^\dagger f_{a1} f_{3b}^\dagger f_{b1} F_{box}^{B_d}[M_a, M_b] \lesssim 3.36 \times 10^{-13} \text{ [GeV]}, \quad (21)$$

$$\Delta m_{B_s} \approx \sum_{a,b=1}^3 f_{3a}^\dagger f_{a2} f_{3b}^\dagger f_{b2} F_{box}^{B_s}[M_a, M_b] \lesssim 1.17 \times 10^{-11} \text{ [GeV]}, \quad (22)$$

$$\Delta m_D \approx \sum_{a,b=1}^3 f_{1a}^\dagger f_{a2} f_{1b}^\dagger f_{b2} F_{box}^D[M_a, M_b] \lesssim 6.25 \times 10^{-15} \text{ [GeV]}, \quad (23)$$

$$F_{box}^M(m_1, m_2) = \frac{m_M f_M^2}{3(4\pi)^2} \int_0^1 \frac{x[dx]}{xm_\chi^2 + ym_1^2 + zm_2^2}, \quad (24)$$

where m_M and f_M are the meson mass and the meson decay constant, respectively. The following parameter values are used in our analysis: $f_K \approx 0.156 \text{ GeV}$, $f_{B_d(B_s)} \approx 0.191(0.274) \text{ GeV}$ [38, 39], $f_D \approx 0.212 \text{ GeV}$, $m_K \approx 0.498 \text{ GeV}$, $m_{B_d(B_s)} \approx 5.280(5.367) \text{ GeV}$, and $m_D \approx 1.865 \text{ GeV}$.

Constraints from direct production of Q' 's: The exotic quarks Q' 's can be produced in pair via QCD processes at the LHC. Each Q' will then decay into $Q' \rightarrow q_i \chi$, where q_i represents a quark with flavor i . Hence, searching for “ $\{tt, bb, tj, bj, jj\}$ + missing E_T ” signals will constrain our present model. The branching ratios for a particular quark flavor i depend on the relative sizes of the Yukawa couplings, f_{3j} and f_{aj} with $a = 1, 2$. We then roughly estimate the lower limit on the mass of Q' using the current LHC data for the s-quark searches [40, 41], which indicates the mass should be larger than $\sim 0.5\text{-}1 \text{ TeV}$ which depends on the mass difference between Q' and χ . In

our following analysis, we simply take the value of $M_a > 1 \text{ TeV}$ in order to satisfy this constraint.

Dark matter : In our model scenario, a complex scalar χ is considered as a DM candidate, since we have a remnant Z_2 symmetry after the $\mu - \tau$ symmetry breaking. The DM candidate and Q'_a are odd under the Z_2 symmetry and the other particles are even. If the M_a is heavier than the m_χ , the DM candidate is a stable particle. The DM dominantly annihilates into the SM leptons via $\chi\chi \rightarrow Z' \rightarrow \mu^+\mu^-(\tau^+\tau^-)$,³ so that the DM in our model is naturally leptophilic. The relic density of the DM is given by

$$\Omega h^2 \approx \frac{1.07 \times 10^9}{\sqrt{g_*(x_f)} M_{Pl} J(x_f) [\text{GeV}]}, \quad (25)$$

where $g^*(x_f \approx 25) \approx 100$, $M_{Pl} \approx 1.22 \times 10^{19}$, and $J(x_f)(\equiv \int_{x_f}^\infty dx \frac{\langle \sigma v_{\text{rel}} \rangle}{x^2})$ is given by

$$J(x_f) = \int_{x_f}^\infty dx \left[\frac{\int_{4m_\chi^2}^\infty ds \sqrt{s - 4m_\chi^2} (\sigma v_{\text{rel}}) K_1\left(\frac{\sqrt{s}}{m_\chi} x\right)}{16m_\chi^5 x [K_2(x)]^2} \right],$$

$$(\sigma v_{\text{rel}}) = \frac{g'^4 q_x^2 s (s - m_\chi^2)}{3\pi [(s - m_{Z'}^2)^2 + m_{Z'}^2 \Gamma_{Z'}^2]},$$

$$\Gamma_{Z'} \approx \frac{g'^2 m_{Z'}}{4\pi} + \frac{|g' q_x|^2}{16\pi m_{Z'}^2} (m_{Z'}^2 - 4m_\chi^2)^{3/2}. \quad (26)$$

With s is a Mandelstam variable, and $K_{1,2}$ are the modified Bessel functions of the second kind of order 1 and 2, respectively. We expect Z' decays into $\mu\bar{\mu}$, $\tau\bar{\tau}$, and $\chi\chi^*$ pairs.⁴ In our numerical analysis, we use the current experimental range for the relic density at 3σ confidential level [29]: $0.11 \lesssim \Omega h^2 \lesssim 0.13$.

Direct detection of DM: The dominant elastic scattering cross section arises from the Q' exchange process in Fig. 3, and its effective Lagrangian of the component level is given by

$$\mathcal{L} \simeq -i \sum_{i=1}^3 \sum_{a=1}^3 \frac{f_{ia}^\dagger f_{ai}}{2M_a^2} [\bar{q}_i \gamma^\mu P_L q_i] [\chi^* \overleftrightarrow{\partial}_\mu \chi], \quad (27)$$

where we use the following assumptions of the four transferred momentum $q^2 = (p_1 - p_2)^2 \ll M_a^2$ and the nucleus of a target almost stops (at rest frame); $\chi^*(p_1)(p_1 - p_2)_\mu \chi(k_1) = \frac{1}{2} \chi^*(p_1) [(p_1 - p_2) + (k_1 - k_2)]_\mu \chi(k_1) \approx \frac{1}{2} \chi^*(p_1)(p_1 + k_1)_\mu \chi(k_1) = \frac{i}{2} \chi^* \overleftrightarrow{\partial}_\mu \chi$, where the right and left sides correspond to the operators in momentum space and spacetime, respectively. We then straightforwardly define the

² We thank Alexander Lenz to bring up a new value of f_{B_s} , which includes a bag parameter dependence.

³ Notice that we do not rely on the Higgs portal, although there are two resonant solutions at around the half masses of the SM Higgs and another neutral Higgs [42].

⁴ Without decay width of Z' , the cross section at around the pole of $2m_\chi = m_{Z'}$ is too large and the relic density would be underestimated.

DM-nucleon elastic scattering operator as follows:

$$\begin{aligned} \mathcal{L}_N \simeq & -i \sum_{i=u}^{d,s} \sum_{a=1}^3 \frac{f_{ia}^\dagger f_{ai}}{4M_a^2} [F_1^{q_i/N} \bar{N} \gamma^\mu N - F_A^{q_i/N} \bar{N} \gamma^\mu \gamma_5 N] \\ & \times (\chi^* \overleftrightarrow{\partial}_\mu \chi), \end{aligned} \quad (28)$$

where we assume that this process is an elastic scattering, then the four transferred momentum is expressed by $q^2 \approx 0$, where p_1 and p_2 are the four momentum of the χ^* and q_i or N , respectively, and $F_{1,A}^{q_i/N}$ are the form factors, which is taken from Ref. [43]. The squared matrix element is given by

$$\begin{aligned} |\mathcal{M}|^2 = & \frac{1}{16} \left| \sum_{i=1}^3 \sum_{a=1}^3 \frac{f_{ia}^\dagger f_{ai}}{M_a^2} (F_1^{q_i/N} \langle N(k_2) | \bar{N} \gamma^\mu N | N(p_2) \rangle \right. \\ & \left. - F_A^{q_i/N} \langle N(k_2) | \bar{N} \gamma^\mu \gamma_5 N | N(p_2) \rangle) \right|^2 \\ & \times |\langle \chi(p_1) | \chi^* \overleftrightarrow{\partial}_\mu \chi | \chi(k_1) \rangle|^2 \\ \simeq & 2m_N^2 m_\chi^2 \sum_{i=1}^3 \sum_{a=1}^3 \left(\left| \frac{f_{ia}^\dagger f_{ai} F_1^{q_i/N}}{M_a^2} \right|^2 + \left| \frac{f_{ia}^\dagger f_{ai} F_A^{q_i/N}}{M_a^2} \right|^2 \right), \end{aligned} \quad (29)$$

where the first and second terms in Eq. (29) do not have an interference term.

Finally, the complete form of the DM-nucleon elastic scattering cross section is expressed by

$$\begin{aligned} \sigma \simeq & \left(\frac{m_\chi m_N}{m_N + m_\chi} \right)^2 \frac{|\mathcal{M}|^2}{32\pi m_\chi^2 m_N^2} \\ = & \frac{1}{16\pi} \left(\frac{m_\chi m_N}{m_N + m_\chi} \right)^2 \\ & \times \sum_{i=1}^3 \sum_{a=1}^3 \left(\left| \frac{f_{ia}^\dagger f_{ai} F_1^{q_i/N}}{M_a^2} \right|^2 + \left| \frac{f_{ia}^\dagger f_{ai} F_A^{q_i/N}}{M_a^2} \right|^2 \right), \end{aligned} \quad (30)$$

where $\sum F_1 \approx 3$ corresponds to the effective operator $(\bar{N} \gamma^\mu N)(\chi^* \overleftrightarrow{\partial}_\mu \chi)$, $\sum F_A \approx 0.49$ corresponds to the effective operator $(\bar{N} \gamma^\mu \gamma_5 N)(\chi^* \overleftrightarrow{\partial}_\mu \chi)$, and $m_N \approx 0.939$ GeV. The current experimental upper bounds for the cross section of the spin independent DM-nucleon elastic scattering are respectively $\sigma_{\text{exp}} \lesssim 2.2 \times 10^{-46} \text{ cm}^2$ at $m_\chi \approx 50$ GeV for the LUX data [32], and $\sigma_{\text{exp}} \lesssim 4.1 \times 10^{-47} \text{ cm}^2$ at $m_\chi \approx 30$ GeV for the XENON data [33]. In our numerical analysis, we conservatively restrict the LUX/XENON1T bounds for the whole range of the DM mass.

III. NUMERICAL ANALYSIS

In this section, results for our numerical analysis are presented. In our analysis, we fix a parameter $|q_\chi| = 1$ for sim-

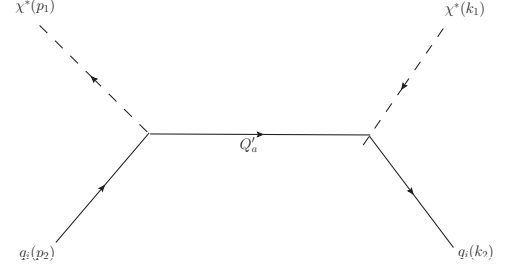


FIG. 3: A Feynman diagram contributing to the spin independent DM-nucleon elastic scattering.

plicity. The ranges of the input parameters are set as follows:

$$\begin{aligned} g' \in [0.1, 1], \quad f \in [0.001, \sqrt{4\pi}], \quad m_{Z'} \in [10, 300] \text{ [GeV]}, \\ m_\chi \in [10, 150] \text{ [GeV]}, \quad M_a \in [1000, 3000] \text{ [GeV]}, \end{aligned} \quad (31)$$

where the lowest DM mass 10 GeV is an assumption to satisfy a condition $(m_\tau/m_\chi)^2 \ll 1$ in the cross section of relic density. In this calculation, we assume $M_1 < M_2 < M_3$, and $m_{Z'} > m_\chi$. We then search the allowed region using the range of the input parameters listed above to satisfy all constraints, namely, $M - \bar{M}$ mixing, the measure of the relic density of the DM, the spin independent DM-nucleon scattering cross section via Z' boson exchange, and the constraint of the LHC as well as to explain the anomaly of $b \rightarrow s\bar{\mu}\mu$ decay.

Fig. 4 shows the allowed region on the plane of m_χ and $m_{Z'}$, where the blue, red, and green dots represent respectively the region corresponding to no constraint on ΔC_9 , 1σ range $-1.29 \lesssim \Delta C_9 \lesssim -0.87$, and 3σ range $-1.67 \lesssim \Delta C_9 \lesssim -0.39$. Note that the lowest point of the maximum absolute value of f is of the order 0.1 for $1(3)\sigma$. The correlation between m_χ and $m_{Z'}$ in Fig. 4 comes from the closed resonant point of the relic density of the DM, when m_χ is heavier. In the lighter region of m_χ , the allowed region becomes wider due to the larger cross section. At around the resonant region of $10 \text{ GeV} \lesssim m_\chi \lesssim 40 \text{ GeV}$, there are no allowed region since the corresponding cross section is too large to satisfy the relic density. This clearly indicates that the mass ranges of the DM and Z' are respectively $10 \text{ GeV} \leq m_\chi \leq 146 \text{ GeV}$ and $10 \text{ GeV} \leq m_{Z'} \leq 295 \text{ GeV}$, where the specific ranges mainly originates from the constraint of the relic density, although the lowest bound of DM mass 10 GeV comes from the lowest input parameter of the DM mass. The anomaly of the decay of $b \rightarrow s\bar{\mu}\mu$ is well explained for the whole allowed region on the plane of m_χ and $m_{Z'}$.

In Fig. 5, we clearly show that the allowed regions on the planes of $\Delta m_K - \Delta m_{B_s}$ (the left panel) and $\Delta m_{B_d} - \Delta m_D$ (the right panel), where the color representation is similar as in Fig. 4. Fig. 5 indicates the allowed region for explaining the anomaly of $b \rightarrow s\bar{\mu}\mu$, which tends to lie in the range of the experimental bounds in our parameter space. A branching ratio of $\text{BR}(b \rightarrow s\gamma)$ is restricted to be 4.02×10^{-4} , but the typical value is at most of the order 10^{-10} . Therefore, the present model clearly satisfies this constraint. Additionally, we found that the LHC constraint tends to be weaker than

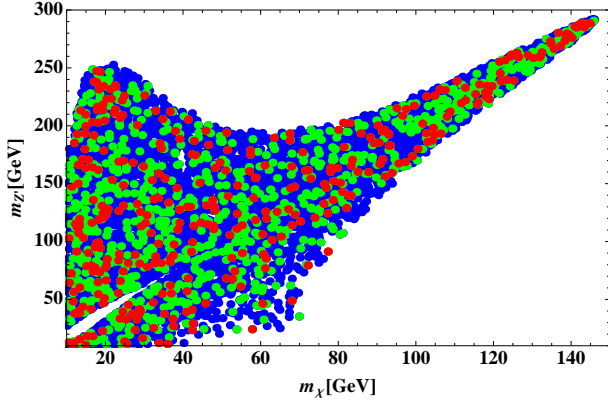


FIG. 4: The allowed region of ΔC_9 on the plane of m_χ and $m_{Z'}$ satisfy the relic density $0.11 \sim 0.13$ and the neutral meson mixings, $b \rightarrow s\gamma$. The blue, red, and green dots are respectively the region of $\Delta C_9 \lesssim -5$, $-1.29 \lesssim \Delta C_9 \lesssim -0.87$ at 1σ , and $-1.67 \lesssim \Delta C_9 \lesssim -0.39$ at 3σ .

the experimental bounds for the neutral meson mixings in our parameter space.

Fig. 6 shows the cross section of the nucleon-DM elastic scattering obtained from our parameter space scanned. This indicates that the parameter points excluded by the present XENON1T data [33]. This means more parameter points can be explored in the future experiments.

IV. SUMMARY AND CONCLUSIONS

We have explored the possibility of explaining the experimental anomalies in the semileptonic decay of the B -meson, $B \rightarrow K^* \mu \bar{\mu}$, in the framework of the gauged $U(1)_{\mu-\tau}$ symmetry. With our present model, which is built in a more complete manner than previous model, we have performed a more detailed analysis by searching the allowed region from several present experimental constraints.

Apart from the muon anomalous magnetic moment and neutrino sector, we have formulated a model starting with a valid Lagrangian by considering the Higgs potential with the inert conditions, the Wilson coefficient for the decay of $B \rightarrow K^* \mu \bar{\mu}$, the collider physics, the neutral meson mixings, the bound on direct detection, and the relic density of a bosonic dark matter candidate. We have searched the parameter space, which explain the size of the anomaly of $B \rightarrow K^* \mu \bar{\mu}$ decay, satisfying all constraints. We found that the allowed region on the plane of the DM and Z' masses is narrower compared to the previous analysis in the heavier DM mass. This is expected due to the decay width of Z' is rather large. On the other hand, in the lighter region of m_χ , the allowed region becomes to be still wider because the cross section is larger. Moreover, there are no allowed region at around the resonant region of $10 \text{ GeV} \lesssim m_\chi \lesssim 40 \text{ GeV}$, since the corresponding cross section is too large to satisfy the relic density. The meson mixing of ΔB_s can be well tested in the future experiments, since the structure of the Yukawa couplings f is the same as the one of ΔC_9 of $B \rightarrow K^* \mu \bar{\mu}$. The absolute parameter of f can naturally be estimated to explain ΔC_9 , and its minimum absolute is at most of the order ~ 0.1 .

Acknowledgments

H.O. was supported by the Ministry of Science, ICT and Future Planning, Gyeongsangbuk-do and Pohang City through the Junior Research Group (JRG) of APCTP. The work of Y.O. was supported from European Regional Development Fund-Project Engineering Applications of Microworld Physics (No.CZ.02.1.01/0.0/0.0/16-019/0000766). The work of P.T.P.H. was supported by the Ministry of Science, ICT and Future Planning, Gyeongsangbuk-do and Pohang City through the Asia Pacific Economic Cooperation-Young Scientist Training (APEC-YST) of APCTP. H.O. is sincerely grateful for the Korea Institute for Advanced Study (KIAS) and all the members.

-
- [1] W. Altmannshofer, S. Gori, M. Pospelov and I. Yavin, Neutrino Trident Production: A Powerful Probe of New Physics with Neutrino Beams, *Phys. Rev. Lett.* **113**, 091801 (2014) [arXiv:1406.2332 [hep-ph]].
 - [2] P. Ko, T. Nomura and H. Okada, Explaining $B \rightarrow K^{(*)} \ell^+ \ell^-$ anomaly by radiatively induced coupling in $U(1)_{\mu-\tau}$ gauge symmetry, *Phys. Rev. D* **95**, no. 11, 111701 (2017) [arXiv:1702.02699 [hep-ph]].
 - [3] G. Arcadi, T. Hugle and F. S. Queiroz, The Dark $L_\mu - L_\tau$ Rises via Kinetic Mixing, *Phys. Lett. B* **784**, 151 (2018) [arXiv:1803.05723 [hep-ph]].
 - [4] T. Nomura and H. Okada, Zee-Babu type model with $U(1)_{L_\mu - L_\tau}$ gauge symmetry, *Phys. Rev. D* **97**, no. 9, 095023 (2018) [arXiv:1803.04795 [hep-ph]].
 - [5] T. Nomura and H. Okada, 'Neutrino mass generation with large $SU(2)_L$ multiplets under local $U(1)_{L_\mu - L_\tau}$ symmetry, *Phys. Lett. B* **783**, 381 (2018) [arXiv:1805.03942 [hep-ph]].
 - [6] S. Lee, T. Nomura and H. Okada, Radiatively Induced Neutrino Mass Model with Flavor Dependent Gauge Symmetry, *Nucl. Phys. B* **931**, 179 (2018) [arXiv:1702.03733 [hep-ph]].
 - [7] S. Baek, H. Okada and K. Yagyu, Flavour Dependent Gauged Radiative Neutrino Mass Model, *JHEP* **1504**, 049 (2015) [arXiv:1501.01530 [hep-ph]].
 - [8] A. Dev, Gauged $L_\mu - L_\tau$ Model with an Inverse Seesaw Mechanism for Neutrino Masses, arXiv:1710.02878 [hep-ph].
 - [9] S. Baek, Dark matter contribution to $b \rightarrow s \mu^+ \mu^-$ anomaly in local $U(1)_{L_\mu - L_\tau}$ model, *Phys. Lett. B* **781**, 376 (2018) [arXiv:1707.04573 [hep-ph]].
 - [10] C. H. Chen and T. Nomura, Neutrino mass in a gauged $L_\mu - L_\tau$ model, arXiv:1705.10620 [hep-ph].
 - [11] K. Asai, K. Hamaguchi and N. Nagata, Predictions for the neutrino parameters in the minimal gauged $U(1)_{L_\mu - L_\tau}$ model,

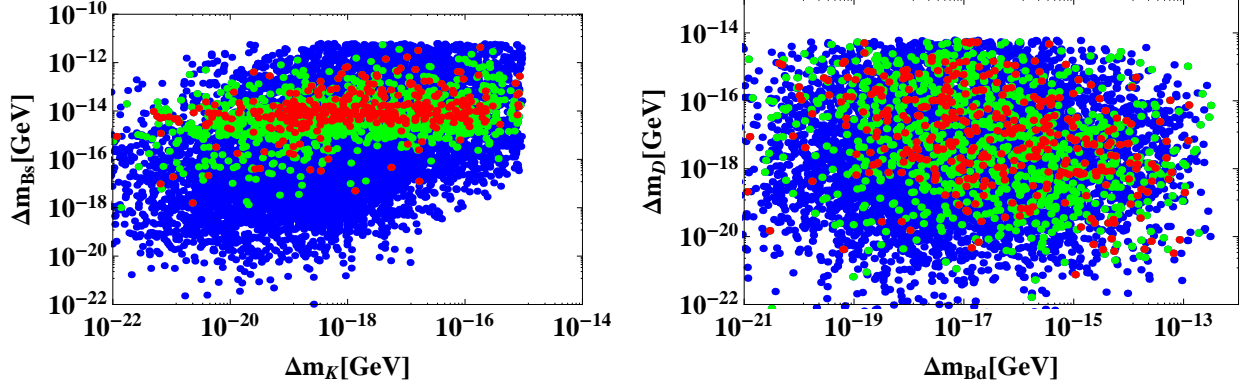


FIG. 5: The allowed region on the $\Delta m_K - \Delta m_{B_s}$ plane (the left panel) and $\Delta m_{B_d} - \Delta m_{B_d}$ plane (the right panel), where the color representations are similar as in Fig. 4.

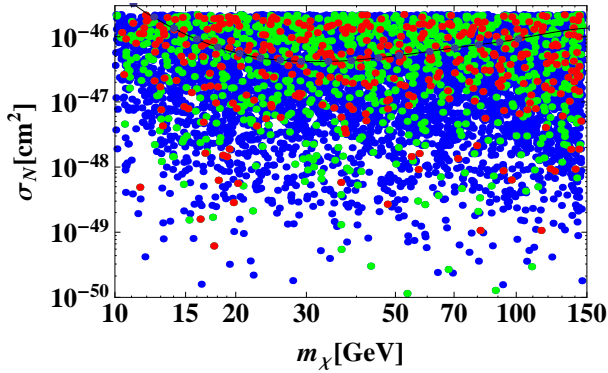


FIG. 6: The nucleon-DM elastic scattering generated by the parameter space scanned. The current upper bound by XENON-1T is represented by the solid line.

- Eur. Phys. J. C **77**, no. 11, 763 (2017) [arXiv:1705.00419 [hep-ph]].
- [12] C. H. Chen and T. Nomura, $L_\mu - L_\tau$ gauge-boson production from lepton flavor violating τ decays at Belle II, Phys. Rev. D **96**, no. 9, 095023 (2017) [arXiv:1704.04407 [hep-ph]].
- [13] A. Biswas, S. Choubey and S. Khan, Neutrino Mass, Dark Matter and Anomalous Magnetic Moment of Muon in a $U(1)_{L_\mu - L_\tau}$ Model, JHEP **1609**, 147 (2016) [arXiv:1608.04194 [hep-ph]].
- [14] S. Baek, Dark matter and muon ($g - 2$) in local $U(1)_{L_\mu - L_\tau}$ -extended Ma Model, Phys. Lett. B **756**, 1 (2016) [arXiv:1510.02168 [hep-ph]].
- [15] K. Asai, K. Hamaguchi, N. Nagata, S. Y. Tseng and K. Tsumura, Minimal Gauged $U(1)_{L_\alpha - L_\beta}$ Models Driven into a Corner, arXiv:1811.07571 [hep-ph].
- [16] H. Banerjee and S. Roy, Signatures of supersymmetry and $L_\mu - L_\tau$ gauge bosons at Belle-II, arXiv:1811.00407 [hep-ph].
- [17] J. Heeck, M. Lindner, W. Rodejohann and S. Vogl, 'Non-Standard Neutrino Interactions and Neutral Gauge Bosons, arXiv:1812.04067 [hep-ph].
- [18] R. Aaij *et al.* [LHCb Collaboration], Angular analysis of the $B^0 \rightarrow K^{*0} \mu^+ \mu^-$ decay using 3 fb^{-1} of integrated luminosity, JHEP **1602**, 104 (2016) [arXiv:1512.04442 [hep-ex]].
- [19] R. Aaij *et al.* [LHCb Collaboration], Measurement of Form-Factor-Independent Observables in the Decay $B^0 \rightarrow K^{*0} \mu^+ \mu^-$, Phys. Rev. Lett. **111**, 191801 (2013) [arXiv:1308.1707 [hep-ex]].
- [20] A. Abdesselam *et al.* [Belle Collaboration], Angular analysis of $B^0 \rightarrow K^*(892)^0 \ell^+ \ell^-$, arXiv:1604.04042 [hep-ex].
- [21] S. Wehle *et al.* [Belle Collaboration], Lepton-Flavor-Dependent Angular Analysis of $B \rightarrow K^* \ell^+ \ell^-$, arXiv:1612.05014 [hep-ex].
- [22] G. Hiller and F. Kruger, More model independent analysis of $b \rightarrow s$ processes, Phys. Rev. D **69**, 074020 (2004) [hep-ph/0310219].
- [23] C. Bobeth, G. Hiller and G. Piranishvili, Angular distributions of $\bar{B} \rightarrow \bar{K} \ell^+ \ell^-$ decays, JHEP **0712**, 040 (2007) [arXiv:0709.4174 [hep-ph]].
- [24] R. Aaij *et al.* [LHCb Collaboration], Test of lepton universality using $B^+ \rightarrow K^+ \ell^+ \ell^-$ decays, Phys. Rev. Lett. **113**, 151601 (2014) [arXiv:1406.6482 [hep-ex]].
- [25] R. Aaij *et al.* [LHCb Collaboration], Test of lepton universality with $B^0 \rightarrow K^{*0} \ell^+ \ell^-$ decays, arXiv:1705.05802 [hep-ex].
- [26] V. Cirigliano, G. Ecker, H. Neufeld, A. Pich and J. Portoles, Kaon Decays in the Standard Model, Rev. Mod. Phys. **84**, 399 (2012) [arXiv:1107.6001 [hep-ph]].
- [27] A. Crivellin, G. D'Ambrosio, M. Hoferichter and L. C. Tunstall, Violation of lepton flavor and lepton flavor universality in rare kaon decays, Phys. Rev. D **93**, no. 7, 074038 (2016) [arXiv:1601.00970 [hep-ph]].
- [28] S. Descotes-Genon, J. Matias, M. Ramon and J. Virto, Implications from clean observables for the binned analysis of $B^- \rightarrow K^* \mu^+ \mu^-$ at large recoil, JHEP **1301**, 048 (2013) [arXiv:1207.2753 [hep-ph]].
- [29] P. A. R. Ade *et al.* [Planck Collaboration], Planck 2013 results. XVI. Cosmological parameters, Astron. Astrophys. **571**, A16 (2014) [arXiv:1303.5076 [astro-ph.CO]].
- [30] D. Aristizabal Sierra, F. Staub and A. Vicente, Shedding light on the $b \rightarrow s$ anomalies with a dark sector, Phys. Rev. D **92**, no. 1, 015001 (2015) [arXiv:1503.06077 [hep-ph]].
- [31] G. Bélanger, C. Delaunay and S. Westhoff, A Dark Matter Relic From Muon Anomalies, Phys. Rev. D **92**, 055021 (2015) [arXiv:1507.06660 [hep-ph]].
- [32] D. S. Akerib *et al.* [LUX Collaboration], Results from a search for dark matter in the complete LUX exposure, Phys. Rev. Lett.

- 118**, no. 2, 021303 (2017) [arXiv:1608.07648 [astro-ph.CO]].
- [33] E. Aprile *et al.* [XENON Collaboration], Dark Matter Search Results from a One Ton-Year Exposure of XENON1T, *Phys. Rev. Lett.* **121**, no. 11, 111302 (2018) [arXiv:1805.12562 [astro-ph.CO]].
- [34] K. A. Olive *et al.* [Particle Data Group], Review of Particle Physics, *Chin. Phys. C* **38**, 090001 (2014).
- [35] S. Descotes-Genon, L. Hofer, J. Matias and J. Virto, Global analysis of $b \rightarrow s\ell\ell$ anomalies, *JHEP* **1606**, 092 (2016) [arXiv:1510.04239 [hep-ph]].
- [36] M. Aaboud *et al.* [ATLAS Collaboration], Search for new high-mass phenomena in the dilepton final state using 36 fb⁻¹ of proton-proton collision data at $\sqrt{s} = 13$ TeV with the ATLAS detector,” *JHEP* **1710**, 182 (2017) [arXiv:1707.02424 [hep-ex]].
- [37] F. Gabbiani, E. Gabrielli, A. Masiero and L. Silvestrini, A Complete analysis of FCNC and CP constraints in general SUSY extensions of the standard model, *Nucl. Phys. B* **477**, 321 (1996) [hep-ph/9604387].
- [38] L. Di Luzio, M. Kirk, and A. Lenz, Updated B_s -mixing constraints on new physics models for $b \rightarrow s\ell^+\ell^-$ anomalies, *Phys. Rev. D* **97**, no. 9, 095035 (2018) [arXiv:1712.06572 [hep-ph]].
- [39] L. Di Luzio, M. Kirk, and A. Lenz, B_s - \bar{B}_s mixing interplay with B anomalies, arXiv:1811.12884 [hep-ph].
- [40] CMS Collaboration [CMS Collaboration], Search for supersymmetry in events with jets and missing transverse momentum in proton-proton collisions at 13 TeV,” CMS-PAS-SUS-16-014.
- [41] M. Aaboud *et al.* [ATLAS Collaboration], Search for squarks and gluinos in final states with jets and missing transverse momentum at $\sqrt{s} = 13$ TeV with the ATLAS detector,” *Eur. Phys. J. C* **76**, no. 7, 392 (2016) [arXiv:1605.03814 [hep-ex]].
- [42] S. Kanemura, S. Matsumoto, T. Nabeshima and N. Okada, ‘Can WIMP Dark Matter overcome the Nightmare Scenario?’, *Phys. Rev. D* **82**, 055026 (2010) [arXiv:1005.5651 [hep-ph]].
- [43] F. Bishara, J. Brod, B. Grinstein and J. Zupan, From quarks to nucleons in dark matter direct detection, *JHEP* **1711**, 059 (2017) [arXiv:1707.06998 [hep-ph]].